Materials Science Forum
ISSN: 1662-9752, Vol. 858, pp 497-500
doi:10.4028/www.scientific.net/MSF.858.497

Submitted: 2015-09-18
Revised: 2015-11-23
Accepted: 2016-01-02
Online: 2016-05-24

Junction Barrier Schottky (JBS) Rectifier Interface Engineering Facilitated by Two-Dimensional (2D) Dopant Imaging

H.R. Rossmann[1,2,a*], U. Gysin[2], A. Bubendorf[2], T. Glatzel[2], S.A. Reshanov[3], A. Zhang[3], A. Schöner[3], T.A. Jung[1,2], E. Meyer[2] and H. Bartolf[4]

[1]Laboratory for Micro- and Nanotechnology, Paul Scherrer Insititute,

CH-5232 Villigen PSI, Switzerland

[2]Department of Physics, University of Basel, Klingelbergstrasse 82, CH-4056 Basel, Switzerland

[3]Ascatron AB, Electrum 207, SE-16440 Kista, Sweden

[4]ABB Switzerland Ltd, Corporate Research, Segelhofstrasse 1K, CH-5405 Dättwil, Switzerland

[a]email: harald.rossmann@psi.ch

Keywords: Two-Dimensional Carrier Profiling, Scanning Probe Microscopy (SPM), Schottky Power Diodes, JBS Rectifier, Wide Band Gap (WBG), Silicon Carbide, Buried Grid (BG)

Abstract. The shielding cell-architecture of a buried grid (BG) Junction Barrier Schottky (JBS) diode consisting of multiple consecutive p^+-implanted stripes below the metal/semiconductor interface has been investigated by performing non-contact Scanning Probe Microscopy (SPM) and Secondary Electron Potential Contrast (SEPC) measurements on device cross-sections. We have shown that these techniques are capable of mapping two-dimensional (2D) carrier distributions inside the active device area, however with different resolution and quantification possibilities.

Introduction

State-of-the-art energy efficient power conversion systems for traction or medium voltage drive applications (*e.g.* 3.3 kV application voltage) require an energy efficient rectifier solution. Such a technology should offer low switching losses during the reverse recovery as well as superior static characteristics such as a low ON-state voltage drop and a low leakage current level in the OFF-state. While SiC Schottky Barrier Diodes (SBD) are able to outperform Si *p-i-n* diodes in terms of switching speed due to their unipolar nature and specific ON-resistance for high breakdown voltages due to the beneficial material properties of SiC, these devices suffer from relatively large leakage currents for reverse-voltages above 1.5 kV [1]. Mainly the almost an order of magnitude higher (as compared to Si) electrical field E at the interface between the carrier-depleted wide band gap material and the Schottky-metal has an undesired impact on the shape of the Schottky barrier $\phi_{B,n}$ which connects the quantum mechanical energy levels of the semiconductor and the metal. Image force induced barrier lowering [2] facilitates thermionic emission for low electric fields while Fowler-Nordheim tunneling [2,3] is the dominant leakage mechanism at high reverse voltages close to avalanche breakdown.

JBS Device Design

The Junction Barrier Schottky (JBS) [4] architecture (Fig. 1) diminishes the influence of the image force by employing highly doped p^+-areas to effectively shield the Schottky-interface from high E-fields. The working principle of this p^+-implanted grid pattern inside the drift layer can be understood as a superposition of reverse biased *p-n* junctions whose depletion fronts merge to sustain high cathode voltages along the whole device. In forward direction this design has two different effects. On the one hand due to the suppression of Schottky-barrier lowering a metal characterized by a lower Schottky-barrier height in contact to the 4H-SiC crystal can be chosen to reduce the ON-state voltage drop, while on the other hand an electron current can only flow between the p^+-regions which leads to an increase of the specific ON-resistance.

Therefore, the tradeoff between the active area consumption of these p^+-grids and their shielding effect has been precisely analyzed and optimized by means of numerical simulations [5]. It was found that the Schottky-contact can be most effectively shielded by narrow and deeply implanted p^+-areas. In this contribution, we investigate a recent descendant of this device architecture, namely the buried grid (BG) JBS design [6]. By shifting the p^+-grid from the surface deeper into the drift layer, a further reduction of both, the electric field E underneath the Schottky-contact and the specific ON-resistance, can be accomplished which is beneficial for the overall device performance. To avoid floating p^+-areas that are sacrificing the surge-current moderation [5,7] offered by biased minority carrier injection, the BG is interconnected trough feeders to the top electrode. However, due to dopant diffusion and activation, the information on the electronically active dopant profile used as input parameter for numerical simulations might change entirely. It is therefore inevitable to map the 2D dopant profile to draw conclusions about the final electronic device performance.

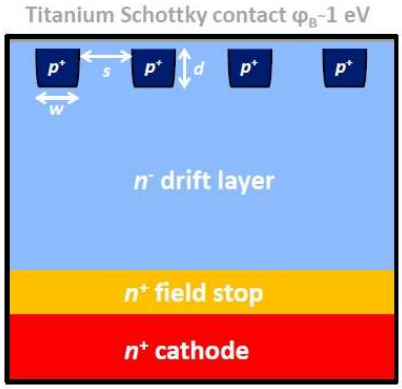

Fig. 1. Schematic view of the sample cross-section of a BG-JBS diode structure. The width w, the spacing s and the depth d of the p^+-implanted regions inside the active area determine the device performance.

Fabrication

The p^+-grid inside the active area of the device was manufactured by cascaded ion implantation of a 1 µm deep box profile (red rectangle in Fig. 2) with an Al concentration in the range of $5 \cdot 10^{19}$ cm^{-3} through a 2 µm thick lithographically patterned SiO_2 hard mask layer. The implantation step was carried out at elevated temperatures of 500°C to prevent crystal amorphization and with the direction of the incident ion-beam perpendicular to the wafer surface. Due to the substrate mis-cut angle of 4° with respect to the crystallographic c-axis, the latter ensures an effective implantation angle which abandons undesired channeling effects. The subsequent activation annealing and epitaxial re-growth can be combined into one processing step, since the parameters are similar (1600-1650°C, 10-15 min). The top 2 µm thick n-type layer has been epitaxially re-grown by using silane-propane chemistry, incorporating nitrogen dopant atoms.

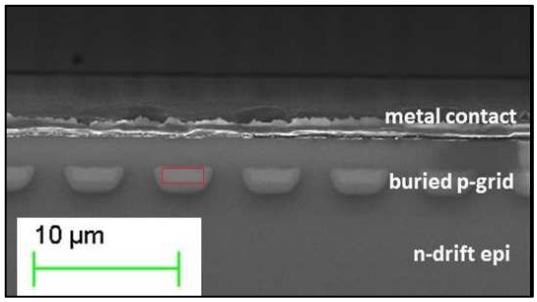

Fig. 2. Electrograph of the sample cross-section of a BG-JBS diode structure. The width w, the spacing s and the depth d of the p^+-implanted regions inside the active area determine the final device performance.

Two-Dimensional Dopant Imaging

In this contribution we utilize complementary dopant observation techniques based either on a commercial Secondary Electron Microscope (SEM) and its ability to map the potential contrast between oppositely doped regions or on a custom-built Scanning Probe Microscope (SPM) [8] which is an even more versatile tool to directly observe dopant concentrations by different physical contrast mechanisms even in the low dopant concentration regime [9].

Cross sections of cleaved BG-JBS structures in 4H-SiC were investigated after a solvent based cleaning process followed by an UV-ozone treatment. Fig. 2 shows the dopant contrast between the p^+-grid inside the n-type drift region, which is a consequence of the band bending in the junction-SEM-system resulting in a different energy spacing with respect to the detector [10]. Impressively, the electrograph clearly resolves the 1 µm deep peak doping concentration as visualized by the bright contrast inside the p^+ JBS cells (Fig. 2). According to Eq. 1,

$$E_{\mathrm{p}} = E_{\mathrm{n}} - qV_{\mathrm{bi}} \tag{1}$$

where $E_{\mathrm{p,n}}$ is the energy required for valence band electrons from p and respectively n doped areas to reach the detector level, q is the elementary charge and V_{bi} is the built in voltage, secondary electrons emitted from the p^{+}-areas require by the amount of $q{\cdot}V_{\mathrm{bi}}$ less energy to reach the detector. Therefore the technique provides better contrast in wide band gap (WBG) semiconductors. Due to the larger secondary electron current these areas appear brighter than the surrounding drift-layer. For an optimized contrast, however, energy filtering to cut-off the high energy tail of the signal has to be applied, which limits the quantification possibilities of this method [10].

On the contrary, raw data collected by non-contact SPM techniques such as Kelvin Probe Force Microscopy (KPFM) [11] and Scanning Capacitance Force Microscopy (SCFM) [12] can be directly utilized to map changes in the oscillatory electrostatic force (ESF) signal with high precision and are therefore offering quantification opportunities. As compared to contact mode, these SPM methods are able to bypass the problem of forming a stable electronic contact due to the immense hardness of SiC. However, also contact mode techniques have been successfully applied to map dopant densities [13]. By means of a lock-in technique separate components of the ESF,

$$F_{\mathrm{esf}} = -\frac{\partial C}{\partial z}\left[\tfrac{1}{2}(V_{\mathrm{dc}} - V_{\mathrm{CPD}})^2 + \tfrac{V_{\mathrm{ac}}^2}{4}\right] - \frac{\partial C}{\partial z}(V_{\mathrm{dc}} - V_{\mathrm{CPD}})V_{\mathrm{ac}}\sin\omega t + \frac{\partial C}{\partial z}\frac{V_{\mathrm{ac}}^2}{4}\cos 2\omega t \tag{2}$$

where C is the tip-sample capacitance, $V_{\mathrm{dc,ac}}$ is the direct and respectively alternating current term of an external bias voltage, $V_{\mathrm{CPD}} = (\phi_{\mathrm{sample}}\text{-}\phi_{\mathrm{tip}})/q$ is the contact potential difference (CPD) and ω is the angular frequency, can be adressed to characterize the electronic properties of the sample.

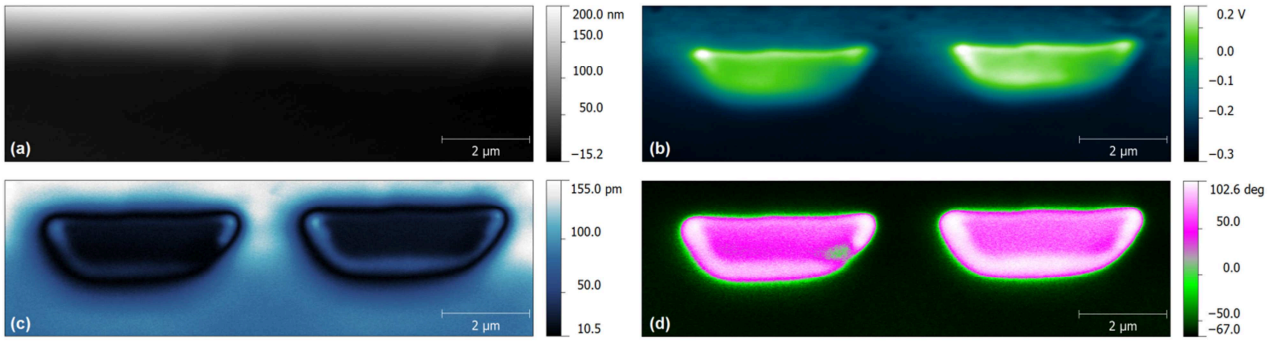

Fig. 3. Comparison of the topography (a), KPFM (b) and SCFM (c,d) images of our sample cross-section. While both methods clearly show the dopant contrast of two adjacent p^{+}-areas, the KPFM image (b) shows a smaller cross section as compared to the amplitude (c) and phase images (d) of SCFM. This can be attributed to the high surface sensitivity of KPFM in contrast to the ~nm information depth of SCFM.

For KPFM, on the one hand, the read out of the dopant dependent CPD can be easily performed by recording the V_{dc} values that are needed to nullify the second term of Eq. 2. The contrast, as shown in Fig. 3, is mainly attributed to a dopant effect since in the topograpic image (Fig. 3a) no well-like structures were observed. However, the junctions in the CPD image (Fig. 3b) are blurried out due to surface defects and adsorbates causing strong band bending. Altough the difference between p-type and n-type regions could be nicely observed and V_{CPD} was found to be ~ 0.38 V, the quantification of these results remains difficult due to the aforementioned undesired surface effects.

On the other hand, SCFM (Fig. 3c,d) is mapping the capacitance variation of the last term of Eq. 2 with respect to an external stimulus. Therefore, the capacitance derivative is expanded into a z and a V dependend contribution [12] and the response of the latter to an ac voltage is investigated. With this method the influence of the doping concentration upon the variable depletion layer capacitance can be studied especially in the low doped regime, since those regions show a higher amplitude signal due to the greater change in the capacitance derivative signal. Hence, the highly doped p^{+}-regions in Fig. 3c appear darker than the lightly doped drift layer. Interestingly, additional features at the border of our structures have been observed. The contrast of these features gets even more pronounced in the SCFM phase image which contains information about the dopant characteristics

(*n* or *p*). According to previous studies [14], we attribute this effect to a bias dependent contrast reversal which is more likely to occur in WBG materials such as 4H-SiC due to their higher interfacial trap density. Similar to KPFM, SCFM is offering a quantification potential as this technique inherently involves local capacitance spectroscopy measurements. However, further theoretical studies are necessary and until now a quantification is only possible by a comparison to precisely gauged calibration samples that were beforehand analyzed by *C-V* measurements [15].

Conclusions

Dopant concentration profiles are designed and manufactured to determine the electronic behavior of every semiconductor device. Notably it is difficult to warrant their 3D distribution within the device during manufacturing and during cyclic use. Here, SPM-derived methods allow for a unique access to dopant profiles along cross-sections of basically every device architecture. The present results on BG-JBS devices in SiC evidence that topographic, capacitive and surface potential contributions regarding the dopant density can be separated and analyzed. The observed differences in the resolution can be attributed to the underlying physical mechanism that is utilized for the observation. While KPFM is a surface sensitive technique that critically depends on the sample preparation, SCFM is probing rather extended depletion layers, therefore averaging out surface-distortions induced by the sample preparation and making it a quite attractive candidate for quantitative dopant mapping. In comparison to SEPC images the two SPM signals exhibit much more quantitative results. However, for routine measurements to observe the profile shape, SEPC provides a quick alternative as compared to SPM-based methods.

In ongoing and future studies, the contrast mechanisms, the resolution and the feasibility of calibrated dopant maps shall be explored. Additionally, different device segments of device architectures at different stages of manufacturing and use provide very interesting specimens to reveal further insights into the atomistic processes in conjunction with dopant implantation and diffusion. Thus, these techniques open up new possibilities to investigate semiconductor and device physics down to the level of ultra-low dopant concentrations and with nanometer scale resolution.

References

[1] K. Asano et al, *Proc. ISPSD 2000*, pp. 97-100 (2000).

[2] S. M. Sze, Physics of Semiconductor Devices (1981).

[3] T. Hatakeyama et al, *Mat. Sci. For*. **433-436**, pp. 831-834 (2003).

[4] B. M. Wilamowski, *Solid State Electron*. **26**, pp. 491-493 (1983).

[5] H. Bartolf et al, *Proceedings of ISPS 2014* edited by V. Benda, CTU Prague, pp. 85-90 (2014).

[6] M. Bakowski et al, *ECS Trans*. **50(3)**, pp. 415-424 (2013).

[7] H. Bartolf et al, *Proc. EPE'15 ECCE*, Geneva, September 2015, in print.

[8] U. Gysin et al, manuscript submitted to *Beilstein J. Nanotechnol*. (2015).

[9] H. Bartolf et al, *Proc. ISPSD 2015*, Hong-Kong, pp. 281-284 (2015).

[10] M. Buzzo, PhD thesis, ETH Zurich (2007).

[11] M. Nonnenmacher et al, *Appl. Phys. Lett*. **58**, 2921 (1991).

[12] K. Kobayashi et al, *Appl. Phys. Lett*. **81**, pp. 2629-2631 (2002).

[13] F. Giannazzo et al, *Mat. Sci. For.* **778-780**, pp. 407-413 (2014).

[14] K. M. Wong et al, *Appl. Phys. Lett.* **87**, 053504 (2005).

[15] H. R. Rossmann et al, *Mat. Sci. For*. **821-823**, pp. 269-272 (2015).

Silicon Carbide and Related Materials 2015
10.4028/www.scientific.net/MSF.858

Junction Barrier Schottky (JBS) Rectifier Interface Engineering Facilitated by Two-Dimensional (2D) Dopant Imaging
10.4028/www.scientific.net/MSF.858.497

DOI References
[2] S. M. Sze, Physics of Semiconductor Devices (1981).
10.1002/9780470068328.fmatter
[4] B. M. Wilamowski, Solid State Electron. 26, pp.491-493 (1983).
10.1016/0038-1101(83)90106-5
[6] M. Bakowski et al, ECS Trans. 50(3), pp.415-424 (2013).
10.1149/05003.0415ecst
[11] M. Nonnenmacher et al, Appl. Phys. Lett. 58, 2921 (1991).
10.1063/1.105227